

## MECHANICAL COMPACTION AND TECTONIC-INDUCED DEFORMATION IN SEDIMENTARY BASINS: MODELING AND TWO-DIMENSIONAL FINITE ELEMENT ANALYSIS

Denise Bernaud<sup>a</sup>, Samir Maghous<sup>b</sup> and Luc Dormieux<sup>c</sup>

<sup>a</sup>CEMACOM, UFRGS, Porto Alegre-RS, Brazil, [bernaud@cpgec.ufrgs.br](mailto:bernaud@cpgec.ufrgs.br)

<sup>b</sup>CEMACOM, UFRGS, Porto Alegre - RS, Brazil, [maghous@cpgec.ufrgs.br](mailto:maghous@cpgec.ufrgs.br)

<sup>c</sup>LMSGC, ENPC, Marne-La-Vallée, France, [dormieux@lmsgc.enpc.fr](mailto:dormieux@lmsgc.enpc.fr)

**Keywords:** sedimentary basin, tectonic loading, finite poroplasticity, finite element method

**Abstract.** In addition to gravitational compaction, tectonic processes represent a major component of deformation in sedimentary basins during diagenesis. The aim of this contribution is to provide theoretical elements for the modeling of these phenomena, together with numerical aspects for basin simulators.

A comprehensive constitutive model for the sediment material is first formulated within the framework of finite poroplasticity. Particular emphasis is put on the effects of large strains on the poromechanical properties of the sediment material.

As regards the numerical assessment of sedimentary basin evolution, an original finite element procedure has been developed, specifically devised for simulating the processes of sediment accretion/erosion.

After the numerical simulation of the whole phases of sediments deposition, the loading originating from tectonic sequences is simulated by imposing horizontal prescribed displacement at the lateral boundaries of the basin. Two-Dimensional (2D) finite element analyses are performed in either compressive tectonics situation.

## 1 INTRODUCTION

Simulation of sedimentary basins with tectonic activity is a complex multidisciplinary problem involving geological, chemical and mechanical aspects. Reconstructing the stress and the deformation history of a sedimentary basin is a challenging and an important problem in geoscience. The potential applications include petroleum exploration, reserve assessment and production.

Many efforts have been done during the past decades as regards the integration of geological data and the simulation of hydrocarbon generation, primary migration, secondary migration and accumulation processes. However, progress in this field has been hampered by the absence of a comprehensive mechanical description of the geological material, which accounts for the strongly coupled nature of the deformation problem. Sedimentary basins form when waterborne sediments in shallow seas are deposited over periods of tens of millions years. The deposited material then compacts under its own weight, causing a reduction of porosity and hence the expulsion of pore fluid. Eventually, as depth increases, chemical reactions occur, such as cementation of granular aggregates and pressure solution. Purely mechanical phenomena prevail in the upper layers, whereas chemical compaction dominates for deeper burial as stress and temperature increase (Schmidt and McDonald, 1979).

Disregarding chemical aspects, the paper will focus on the modeling of purely mechanical compaction with tectonic activity.

The basic models of mechanical compaction are still based on phenomenological relationships relating porosity to effective vertical stress. The concept of porosity versus Terzaghi's effective stress dependence has been early introduced by Hubert and Rubey (1959) and later by Smith (1971). These ideas have been widely adopted and implemented in numerical finite element models that have yielded valuable contributions to the understanding of the evolution of sedimentary basins.

Still, a more comprehensive description of the mechanics involved in basin simulation should be achieved within the tensorial formalism of the constitutive model. This is necessary for addressing the boundary conditions encountered in the case of tectonic activity, or for the determination of the horizontal stresses induced by the compaction phenomenon. The main difficulty rises from the large porosity changes involved in compaction problem. This requires that the poromechanical constitutive law be formulated in the framework of finite irreversible strains (see for example Tuncay et al. (2000); Bourgeois and Dormieux (1997); Deudé et al. (2004) or Barnichon and Charlier (1996)).

The coupled nature of the deformation problem may be understood as follows. Large

strains modify the microstructure, microstructure modifications lead to a change in the poromechanical properties of the sediment material, which in turn affect the basin response. Theoretical formulation accounting for the effects of the porosity changes on the elastic and plastic properties of the porous material have been proposed in Dormieux and Maghous (2000); Bernaud et al. (2002); Barthélémy et al. (2003) and Deudé et al. (2004). It is shown in particular that the time dependence of poroelastic parameters with large plastic strains leads to additional terms in the constitutive equations.

In Bernaud et al. (2006), the problem of purely gravitational compaction, including explicit simulation of distinct phases of sediments depositions, has been addressed within the framework of finite element method in finite poroplasticity. The main objective of this contribution is to extend the analysis to account for tectonic-induced deformation in sedimentary basins during diagenesis.

It is well established that the deformation evolution and associated poromechanical state of sedimentary basins are significantly affected by all the tectonic processes occurring during their life-cycle. For instance, extensional sedimentary basins that are subjected to shortening may experience uplift of basin sediments and reverse reactivation of faults in a process which is referred to as basin inversion.

Few works are dedicated in the recent literature to theoretical or numerical modeling of these phenomena. A numerical simulation was proposed in Hutton and Syvitski (2003) making use the computer 2D program SedFlux which was modified to simulate the distribution of seafloor geotechnical parameters during the growth of a seismically active continental margin. The mechanics of tectonic inversion of the Pannomian has been investigated by Jarosinski et al. (2009) using the FEM code ANSYS. The authors modeled the sediments behavior by a means of a Mohr-Coulomb law which is capable to couple elasticity, viscous and plastic strains and temperature. Buitter et al. (2009) studied the inversion of extensional sedimentary basins through a numerical evaluation of the localization of shortening; the modeling consists of a thermo-mechanical constitutive law with a Drucker-Prager criterion. Zhao et al. (2000) developed a finite element model to simulate the fluid rock interaction in pore-fluid saturated hydrothermal sedimentary basins.

Three-dimensional basin modeling software is now routinely used in commercial petroleum exploration. However, very little has been published about the formulation, discretization and solution of these models. Mello et al. (2009) describe a 3D control-volume finite-element method to solve numerically the coupled partial differential equations governing geological processes involved in the evolution of sedimentary basins. These processes include sediment deposition and deformation, hydrocarbon generation, multiphase fluid flow and heat transfer in deforming porous media.

The analysis is focused in this paper on the modeling of tectonic activity within the theoretical framework of large poroplastic strains previously formulated in Bernaud et al. (2006). After the entire phase of sediment accretion, the sedimentary basin is submitted to extensional /compressive tectonic which are superposed to gravitational compaction and pore pressure dissipation processes.

## 2 THEORETICAL ASPECTS

During compaction process, the particles of the porous material (i.e. sediment material) are subjected to large volumetric strains: the porosity change may reach 50% as the burial goes on. Appropriate prediction of the basins response should thus take into account both the constitutive non linearities and the geometric non linearities induced by large strains.

### 2.1 State equations and complementary relations

At the scale of pores and solid grains, large strains modify the microstructure of the sediment material. In turn, these microstructural changes are responsible for the evolution of elastic and plastic mechanical properties.

The sedimentary rock is modeled as a fully saturated poroelastoplastic material undergoing large strains. The anisotropy of the mechanical properties of the sedimentary material induced by compaction is disregarded. The elastic part of the deformation gradient of the skeleton particles is assumed to remain infinitesimal. This means that large strains involved during compaction process are of irreversible (plastic) nature.

In the framework of finite poroplasticity, the constitutive behavior comprises two state equations in rate-type formulation together with complementary relations specifying the flow rule (Dormieux and Maghous, 2000; Bernaud et al., 2002; Bernaud et al., 2006). Let  $\underline{\underline{\sigma}}$  denotes the Cauchy stress tensor and  $p$  the pore pressure. The first state equation relates the stress rate  $\underline{\underline{\dot{\sigma}}}$ , the pore pressure rate  $\dot{p}$ , and the strain rate tensor  $\underline{\underline{d}}$  defined as the symmetric part of the velocity gradient:

$$\frac{D_j \underline{\underline{\sigma}}}{Dt} = \underline{\underline{\dot{\sigma}}} + \underline{\underline{\sigma}} \cdot \underline{\underline{\Omega}} - \underline{\underline{\Omega}} \cdot \underline{\underline{\sigma}} = \underline{\underline{\zeta}} : (\underline{\underline{d}} - \underline{\underline{d}}^p) + \underline{\underline{\zeta}} : \underline{\underline{\zeta}}^{-1} : \underline{\underline{\sigma}} \quad (1)$$

where  $\underline{\underline{d}}^p$  denotes the plastic strain rate while  $\underline{\underline{\Omega}}$  is the rotation (spin) rate tensor which

aims at taking the large rotation of the elementary volume into account. This equation involves:

- a rotational time derivative of the Biot effective stress tensor  $\underline{\underline{\sigma}}^e = \underline{\underline{\sigma}} + b p \underline{\underline{1}}$  where  $b$  is the Biot coefficient;
- a term related to the particulate derivative  $\dot{\underline{\underline{c}}}$  of the tensor of drained elastic moduli  $\underline{\underline{c}}$ .

The evolution of the elastic properties is related to those of the microstructure which cannot be neglected in the domain of large strains. Relationship (1) extends classical rate form formulations (Meroi et al., 1995; Bourgeois and Dormieux, 1997; Dormieux and Maghous, 1999) to the case of variable elastic properties.

The second state equation relates the pore volume change to the rate  $\dot{p}$  of the pore pressure and to the strain rate  $\underline{\underline{d}}$ . Let  $J$  and  $J^p$  denote the jacobian of the transformation of the elementary volume and its plastic part, respectively. The rates  $\dot{J}$  and  $\dot{J}^p$  are given by:

$$\dot{J} = J \operatorname{tr} \underline{\underline{d}} \quad \text{and} \quad \dot{J}^p = J^p \operatorname{tr} \underline{\underline{d}}^p \quad (2)$$

With these notations, the rate form of the second state equation reads (Bernaud et al., 2002):

$$\dot{p} = M \left( -b \operatorname{tr} \left( \underline{\underline{d}} - \underline{\underline{d}}^p \right) + \frac{\dot{\phi} - \dot{\phi}^p}{J^p} \right) + \frac{\dot{M}}{M} p - M \dot{b} \operatorname{tr} \left( \underline{\underline{c}}^{-1} : \underline{\underline{\sigma}}^e \right) \quad (3)$$

$\phi$  is the lagrangian porosity,  $\phi^p$  the corresponding plastic part and  $M$  is the Biot modulus.

The terms involving  $\dot{M}$  and  $\dot{b}$  in (3) are related to the influence of large plastic strains on the poroelastic properties.

The complementary equations prescribe the plastic flow rule. Generalizing the concept of plastic potential, we therefore introduce the function  $g(\underline{\underline{\sigma}}, p)$  which derivatives yield the sought plastic rates:

$$\underline{\underline{d}}^p = \chi \frac{\partial g}{\partial \underline{\underline{\sigma}}} ; \quad \dot{\phi}^p = J^p \chi \frac{\partial g}{\partial p} \quad (4)$$

where  $\chi$  is a non-negative plastic multiplier.

The plastic incompressibility of the solid phase is assumed in the sequel. This implies that the plastic part of the pore volume change is identical to the plastic part of the total volume change and yields  $\dot{\phi}^p = \dot{J}^p$ . Owing to (20), it is further obtained that  $\dot{\phi}^p = J^p \operatorname{tr} \underline{\underline{d}}^p$ .

Combining this equation with (4) reveals that the plastic potential depends on  $\underline{\underline{\sigma}}$  and through the so-called Terzaghi effective stress  $\underline{\underline{\sigma}}' = \underline{\underline{\sigma}} + p \underline{\underline{1}}$  (e.g. Bourgeois et al., 1995):

$$g(\underline{\underline{\sigma}}, p) = \Psi(\underline{\underline{\sigma}}') ; \quad \underline{\underline{d}}^p = \dot{\chi} \frac{\partial \Psi}{\partial \underline{\underline{\sigma}}'} \quad (5)$$

The relevancy of the above model depends on the capability to specify:

- the elastic-plastic coupling characterized by the dependence of tensor  $\underline{c}$  as well as poroelastic coefficients  $b$  and  $M$  on large plastic strains;
- the influence of large plastic strains on the evolution of the yield surface as well as on the hardening rule.

## 2.2 Influence of microstructural changes on poroelastic and hardening properties

In the case of plastic incompressibility of the solid matrix, large plastic strains of porous material are expected to induce significant porosity and pore shape changes. In order to capture the influence of the plastic strains on the poroelastic properties, the idea is to resort to micromechanical estimates of the latter. For the sake of simplicity, the anisotropy induced during the loading process is disregarded in this study. The pore space is therefore entirely characterized by its volume fraction, namely the eulerian porosity  $\varphi = \phi / J$ . We herein adopt the Hashin-Shtrikman upper bounds which are known to reasonably model the elastic properties of isotropic porous media (see for instance Zaoui, 2002). Accordingly, the bulk moduli  $K$  and the shear moduli  $\mu$  of the porous medium now appear as functions of the porosity as well as of the elastic properties of the solid phase (that are assumed to be constant):

$$K(\varphi) = \frac{4k^s \mu^s (1-\varphi)}{3k^s \varphi + 4\mu^s}; \quad \mu(\varphi) = \frac{\mu^s (1-\varphi)(9k^s + 8\mu^s)}{k^s (9 + 6\varphi) + \mu^s (8 + 12\varphi)} \quad (6)$$

where  $k^s$  and  $\mu^s$  are the bulk and the shear moduli of the solid phase. It is recalled that the Biot coefficient and modulus are connected to  $K$  through:

$$b(\varphi) = 1 - \frac{K(\varphi)}{k^s} \quad \text{and} \quad \frac{1}{M(\varphi)} = \frac{b(\varphi) - \varphi}{k^s} \quad (7)$$

We now need to relate the porosity change to the plastic strains undergone by the porous material. To do so, we first observe that the condition of plastic incompressibility of the solid constituent reads:

$$J^p - \phi^p = 1 - \varphi_0 \quad (8)$$

where  $\varphi_0$  denotes the initial value of the porosity. In the framework of infinitesimal elastic

strains, it is possible to neglect the variation of the pore volume and that of the total volume between the loaded and unloaded configurations of the elementary volume, since these variations are reversible by definition. This justifies the following approximations:

$$J^p \approx J \quad \phi^p \approx \phi \quad (9)$$

Introducing (9) into (8) yields:

$$\varphi \approx 1 - \frac{1 - \varphi_0}{J} \approx 1 - \frac{1 - \varphi_0}{J^p} \quad (10)$$

In view of (10), equation (6) shows that the macroscopic stiffness tensor  $\underline{c}$  is a function of the (total or plastic) jacobian:  $\underline{c} = \underline{c}(J^p)$ . The same conclusion holds for the poroelastic coefficients  $b$  and  $M$ . Neglecting the induced anisotropy therefore amounts to the fact that the elastic-plastic coupling properties are only governed by the plastic volumetric strains.

As regards the evolution of the plastic properties of the porous medium, it is first assumed that the yield surface  $f$  is that of the standard modified Cam-Clay (Muir Wood, 1990):

$$f(\underline{\underline{\sigma}}' = \underline{\underline{\sigma}} + p\underline{\underline{1}}, p_c) = \frac{3}{2} \underline{\underline{s}} : \underline{\underline{s}} + M_{cs}^2 p'(p' + p_c) \quad (11)$$

where  $\underline{\underline{s}} = \underline{\underline{\sigma}} - \frac{1}{3} tr \underline{\underline{\sigma}} \underline{\underline{1}}$  is the deviatoric stress tensor and  $p' = \frac{1}{3} tr \underline{\underline{\sigma}}'$  is the mean effective stress.  $p_c$  is the consolidation pressure and represents the hardening parameter of the model. The constant  $M_{cs}$  is the slope of the critical state line. The plastic flow rule is associated, i.e.  $g = f$ .

The hardening law, that is the influence of large plastic strains on the consolidation pressure, is a crucial feature of the model. In the framework of the Cam-clay model, the standard hardening law may be written in the domain of large strains

$$p_c(J^p) = p_{c0} e^{-\alpha(J^p - 1)} \quad (12)$$

where  $\alpha$  is a material constant.

However, such a hardening law does not enforce the condition  $J^p > 1 - \varphi_0$ , corresponding to total pore closure (see (10)). It is therefore expected that a simple extension of the classical Cam-Clay hardening law in the form (12) might yield negative porosities under high isotropic compression. That is of course not satisfactory. Instead of (12), we shall hereafter resort to a micromechanical approach to the hardening law which overcomes the above difficulty. The idea is to identify  $p_c(J^p)$  to the limit load of a hollow

sphere subjected to isotropic compression in the domain of large strains. In fact, as early noticed by Hashin, the hollow sphere is the simplest conceptual model for an isotropic porous medium. Considering the case of a solid phase of the Tresca type, the limit load appears to be a function of the current porosity  $\varphi$  (pore volume fraction):

$$p_c(J^p) = \frac{p_{c0}}{\ln \varphi_0} \ln\left(1 - \frac{1 - \varphi_0}{J^p}\right) \quad (13)$$

As opposed to (12), we note that the consolidation pressure predicted by (13) tends towards infinity when the pore space vanishes. This is the way that this micromechanics-based hardening law avoids the development of negative porosities.

### 2.3 Finite element analysis

Consider a material system defined by porous medium which occupy a geometrical domain  $\Omega$ . Within the framework of finite poroplasticity, the quasi-static boundary value problem is defined on  $\Omega$  by:

- the momentum balance equation:

$$\text{div} \underline{\underline{\sigma}} + \rho \underline{\underline{g}} = \underline{\underline{0}} \quad (14)$$

- the fluid mass balance equation:

$$\dot{\rho}^f \varphi + J \text{div} \rho^f \underline{\underline{q}} = 0 \quad (15)$$

where  $\rho^f$  is the fluid density and  $\underline{\underline{q}}$  is the filtration vector. The latter is connected to the fluid pressure through the Darcy's law:

$$\underline{\underline{q}} = \underline{\underline{k}} \cdot (-\nabla p + \rho^f \underline{\underline{g}}) \quad (16)$$

$\underline{\underline{k}}$  denotes the permeability tensor. In the case of isotropy (i.e.  $\underline{\underline{k}} = k \underline{\underline{1}}$ ), effects of microstructural changes on the evolution of  $\underline{\underline{k}}$  may be modeled by means of Kozeny-Carman formula:

$$k = k_0 \frac{\varphi^3 (1 - \varphi_0)^2}{\varphi_0^3 (1 - \varphi)^2} \quad (17)$$

$k_0 = k(\varphi_0)$  is the initial value of the permeability.

- the constitutive equations.

Within the framework of finite poroplasticity, the latter are given by (1) and (3) together with the plastic flow rules (5). The elastic moduli, the yield surface and the hardening law are described by (6-7), (11) and (13), respectively. In addition, the initial conditions must be specified as well as the mechanical and hydraulic boundary conditions.

It must be emphasized that all equations defining the boundary value problem refer to the mechanical system in its current configuration, which is a priori unknown.

The finite element analysis will be outlined hereafter. Fully details are given in Bernaud et al. (2002).

The updated Lagrangian scheme (Bathe, 1996) is used in order to analyze the large strain behaviour of the structure under consideration. In this approach, all static and kinematic variables are referred to an updated configuration in each step time  $\Delta t$ . Denoting by  ${}^t \underline{x}$  the coordinates of any skeleton particle in the configuration of the mechanical system at time  $t$ , it is convenient to reformulate the problem in terms of the displacement between  $t$  and  $t + \Delta t$ :

$$\underline{U} = {}^{t+\Delta t} \underline{x} - {}^t \underline{x} \quad (18)$$

and of the pore pressure values difference  $P$  at points similar within the skeleton transformation at times  $t$  and  $t + \Delta t$ :

$$P = p(x)^{t+\Delta t} - p(x)^t \quad (19)$$

The weak forms of the equilibrium and fluid mass balance equations, expressed at time  $t + \Delta t$ , are derived. A standard 2D finite element formulation employing 6-nodes triangle elements is used. The components of the displacement  $\underline{U}$  are approximated by a quadratic polynom function of the 6 nodal values. The approximation of the pressure  $P$  is linear with corresponding nodes located at the three summits of the triangle. This procedure yields to the following matrix equation:

$$\begin{bmatrix} K_{UU} & K_{PU} \\ K_{UP} & K_{PP} \end{bmatrix} \begin{bmatrix} \underline{u} \\ \underline{p} \end{bmatrix} = \begin{bmatrix} \underline{F}_U \\ \underline{F}_P \end{bmatrix} \quad (20)$$

where  $K_{IJ}$  and  $\underline{F}_I$  are the global stiffness sub-matrices and force sub-vectors, respectively.  $\underline{u}$  and  $\underline{p}$  are the global vectors whose components are node values of the displacement

$\underline{U}$  and the pressure  $P$ , respectively.

Consequently, the above system of equations is nonlinear because of the dependence of  $\underline{F}_U$  and  $\underline{F}_P$  on  $\underline{u}$  and  $\underline{p}$ . For this reason, at each time, it is necessary to solve (20) by an iterative algorithm until (20) is satisfied up to a required tolerance.

Explicit expression for matrices  $K_{II}$  and vectors  $\underline{F}_I$  together with the description of the iteration procedure are given in Bernaud et al. (2002).

### 3 NUMERICAL PROCEDURE

The specificity of the numerical simulation of sedimentary basins lies in the fact that the system under consideration is an open system. Consequently, appropriate numerical approaches such as finite element one must implement appropriate procedures to model continuous sediment supply.

The numerical approach used in this study, which is aimed to simulate the time evolution of the basin boundary, is based upon a technique directly inspired from tunnel engineering. It is explained in Bernaud et al. (2006).

The basin undergoing compaction is modeled as an horizontal infinite layer (Fig. 1). The basement rock is located at  $z = 0$ . Assuming it remains horizontal, the upper boundary is defined by the time dependent plane equation  $z = H(t)$ , where  $H(t)$  refers to the total thickness of the basin at time  $t$ . Besides, the sea level is located at the plane  $z = L_0$ .

These geometrical assumptions are adopted for simplicity. Nevertheless, more complex 2D basin geometries can also be handled by means of our numerical code.

In absence of tectonic activity, the gravity forces  $-g\underline{e}_z$  and the fluid pressure at the top of the basin constitute the loading parameters in the compaction process. If  $\rho(z, t)$  denotes the mass density of the sediment material, the mass sediments supplied per unit area from the initial time  $t = 0$  is equal to that of the vertical column with unit cross section:

$$M_d(t) = \int_0^{H(t)} \rho(z, t) dz \quad (21)$$

The boundary conditions consist in prescribing the values of the stress vector  $\underline{T} = \underline{\underline{\sigma}} \cdot \underline{e}_z$ , displacement vector  $\underline{\xi}$ , fluid pressure  $p$  and the fluid flux  $\underline{q} \cdot \underline{e}_z$ :

\*  $z = H(t)$  (upper surface)

$$\underline{T} = -\rho^f g(L_0 - H(t))\underline{e}_z \quad , \quad p = \rho^f g(L_0 - H(t)) \quad (22)$$

\*  $z = 0$  (basin basement)

$$\underline{\xi} = 0 \quad , \quad \underline{q} \cdot \underline{e}_z = 0 \quad (\text{impermeability condition}) \quad (23)$$

The numerical technique (for more details see Bernaud et al. (2006)) to simulate the sedimentary basin consists in transforming the real open material system (the basin) into a fictitious closed system. The evolution in time of the latter must of course correspond to that of the real system. The main advantage of this procedure lies in the fact that the finite element approach briefly described in section 2.3 is applicable.

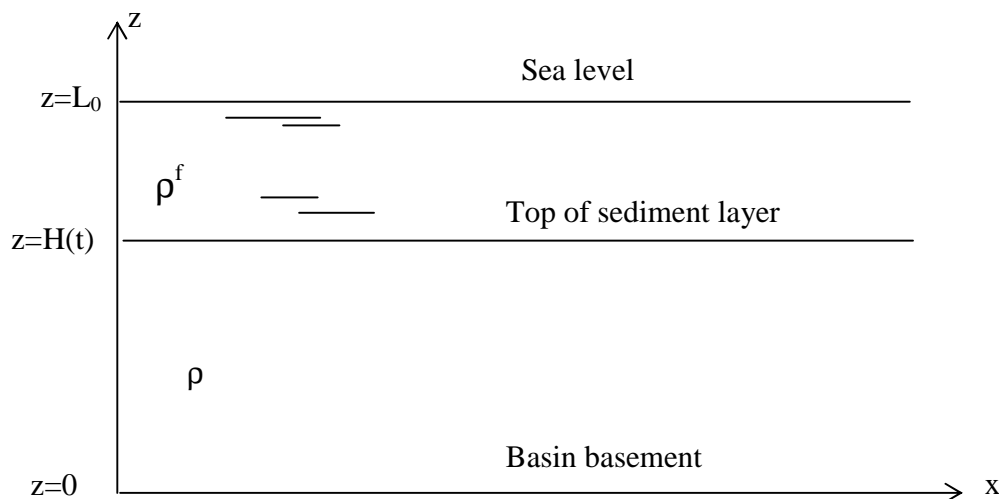


Figure 1: Schematic geometry of the basin.

#### 4 GRAVITATIONAL COMPACTION SIMULATIONS

The basin deformation model described in the previous sections has been implemented in a two-dimensional finite code.

Before studying the basin under tectonic activity, we first proceed to the simulation of the sedimentary basin formation (i.e., construction of the basin). This is achieved by means

of the numerical technique briefly explained in section 3.

The first step of basin simulation (prior to tectonic loading application) is carried out within a 2D setting. Oedometric conditions are assumed for the modeling. Even a 1D setting would be sufficient for this task, a 2D modeling of the basin geometry proves to be necessary in the perspective to proceed, sequentially to the construction of the basin, to the analysis of basin tectonics induced-deformation. The initial geometry of the fictitious system considered for calculations is displayed in Fig. 2. It is defined by a rectangular block of 24 km long by  $H = 6$  km thick. Owing to the symmetry with respect to the vertical plane, only the half part  $0 \leq x$  of the initial geometrical domain is discretized into finite elements. The finite element mesh consists in 7200 triangular elements (each triangle is viewed as T6 for displacement interpolation and as T3 for pore pressure interpolation) regularly distributed along 120 horizontal layers, each layer being divided into 60 elements. The mesh corresponds to 14701 total nodes.

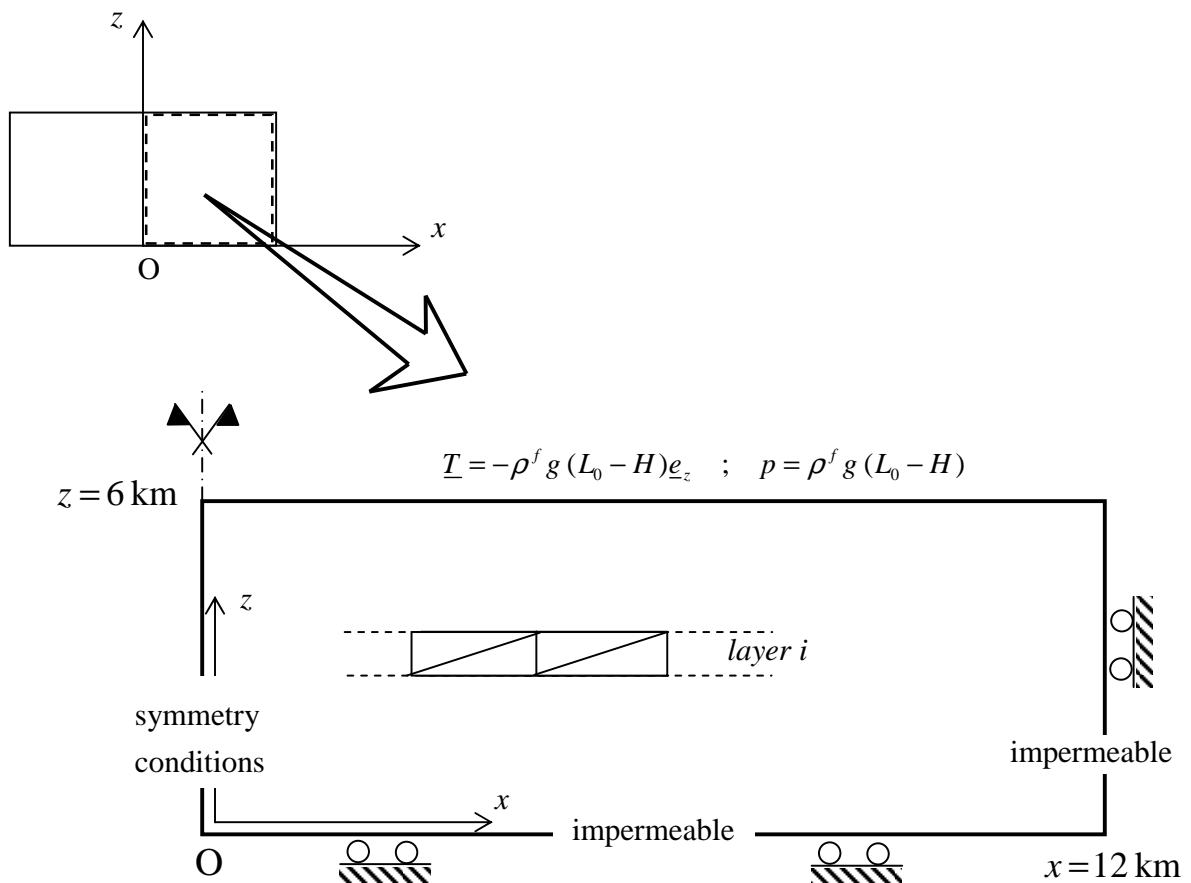


Figure 2: Initial geometry model: dimensions and boundary conditions.

The simulations carried out in the subsequent analysis assume the following characteristics:

- (a) The yield surface is that of the standard modified Cam-Clay (11).
- (b) The sediment material supplied at the top of the basin is assumed to have constant mechanical and hydraulic properties at the geologic time scale.
- (c) The accretion rate  $\dot{M}_a$  is constant at the geologic time scale.
- (d) The basin is made up of an amount of material supply which would correspond to a vertical column of thickness  $H = 6000$  m in absence of compaction or in other words if the sediment material were rigid. The sea level is 2000 m higher at the top of the basin, which means that the column of sea water has  $L_0 = 8000$  m.

In addition, the following material parameters have been adopted for the calculations: Initial material density  $\rho_0 = 1.37 \times 10^3$  kg/m<sup>3</sup>, initial porosity  $\phi_0 = 0.72$  (data taken from Hamilton, 1959), fluid density  $\rho^f = 10^3$  kg/m<sup>3</sup>, initial Young modulus  $E_0 = 10^3$  MPa, initial Poisson's ratio  $\nu_0 = 0.33$ , initial Biot coefficient  $b_0 = 0.9715$ , initial Biot modulus  $M_0 = 1.392 \times 10^5$  MPa, coefficient slope of the critical state line  $M_{cs} = 1.2$ , permeability  $k_0 = 10^{-10}$  MPa<sup>-1</sup> x m<sup>2</sup> x s<sup>-1</sup>, initial consolidation pressure  $p_{c0} = 1.5$  MPa. The rate of sediments supply corresponds to an increase in the layer thickness of 100 m per million years (Myr), if no deformation occurs.

Figure 3 illustrates the compaction curve of the basin versus the time. The entire construction of the sedimentary basin takes 60 millions years when the column presents the height of  $H(t) = 4212$  m, instead of  $H(t) = 6000$  m if no deformation occurs. During the phase of basin formation (phase of accretion  $t \leq 60$  Myr) the deformation of the basin is mainly controlled by gravity compaction. After its total construction (i.e., after the process of sediment accretion has stopped  $t > 60$  Myr), the deformation is mainly due to the process of pore pressure dissipation. The complete stabilisation of deformations is reached after approximately 1600 millions years, and the corresponding final height of the basin is  $H(t) = 2690$  m.

The numerical results of the basin simulation at  $t=60$  millions years will be the initial state for the tectonic numerical calculations. It means that for the tectonic calculation activated at  $t=60$  Myr, the initial Young's modulus take the values given in figure 3, the initial hardening parameter is given by the values of figure 4 and the initial porosity is given by the values of figure 5. It means that several parameters of the problem are function of the depth of the layer.

For the time  $t = 60$  Myr, figure 4 illustrates the variation of the Young's Modulus with the layer depth. We can observe that as expected the Young's modulus presents its maximum value  $E=4800$  MPa at the basement of the basin; at the top of the model the

Young's modulus presents the value of the initial calculation  $E = 1000$  MPa.

The variation of the consolidation pressure (Fig. 5), which represents the hardening parameter of our model, has the same form of the curve of the Young's modulus: the maximum value  $p_{c0} = 4.5$  MPa occurs at  $z = 0$ , and the minimum  $p_{c0} = 1.5$  MPa is in the zone near the top of the basin.

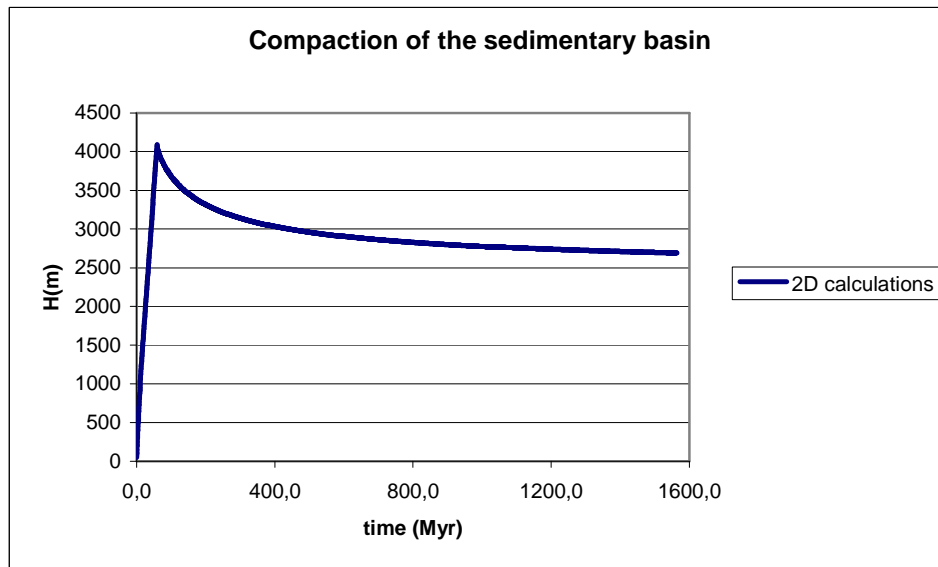


Figure 3: Compaction law of the sedimentary basin.

The fluid pressure predicted by the numerical model at  $t = 60$  Myr is reported in Fig. 6. During sediments deposition ( $t \leq 60$  Myr), the pore pressure is a decreasing function with a maximum value reached at the bottom.

The porosity decreases with the depth of the layers as it is illustrated in figure 7: the porosity is equal to about 0.17 at the basement of the basin and it is equal to 0.72 near the top of the basin.

## 5 FINITE ELEMENT SIMULATIONS OF TECTONIC SEQUENCES

A simplified 2D framework is adopted herein to simulate tectonic sequences acting on the sedimentary basin during the process of compaction. As often made (see for instance Mantovani et al. (2000); Strayer et al. (2001); Frederiksen et al. (2001) or Babeyko (2002)), the tectonic regime is modeled by means of prescribed velocity boundary conditions. The

numerical calculations are performed using the fully poroplastic coupled constitutive model presented in section 2 under plane strains conditions parallel to the plane  $(x, z)$ .

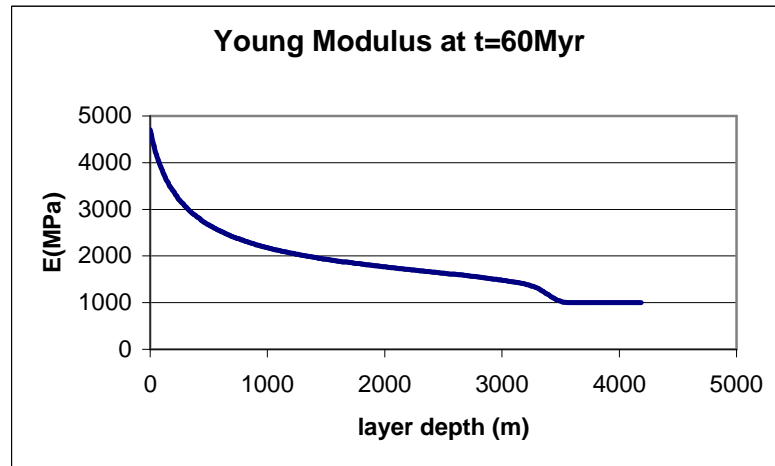


Figure 4: Young's modulus versus layer depth at  $t=60\text{Myr}$ .

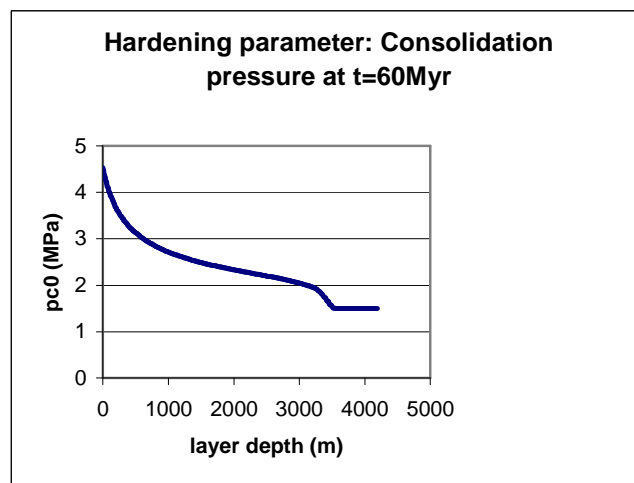


Figure 5: Consolidation pressure versus layer depth at  $t=60\text{Myr}$ .

### 5.1 Model geometry and boundary conditions

We proceed as follows. Once the phase of sediment deposition  $0 \leq t \leq 60 \text{ Myr}$  is simulated, the tectonic loading is applied from time  $T = 60 \text{ Myr}$  and increasing the value of the horizontal displacement imposed at the lateral sides of the basin as the time increases.

The geometry and hydromechanical fields (stress, pore pressure, porosity and associated poromechanical parameters) at  $t = 60$  Myr are considered as initial configuration and state of the basin when starting the tectonic loading. This means in particular that application of the initial configuration for tectonic loading is characterized by basin thickness  $H(T = 60 \text{ Myr}) = 4212 \text{ m}$  (Fig. 8) resulting from deformation during sediments accretion phase a highly pre-stressed state and a pore pressure profile which is far from hydrostatic distribution.

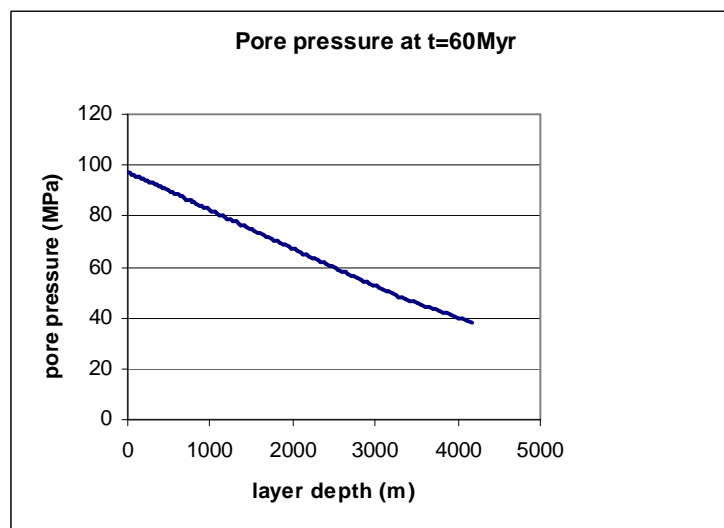


Figure 6: Pore pressure profile along the basin at  $t=60$ Myr.

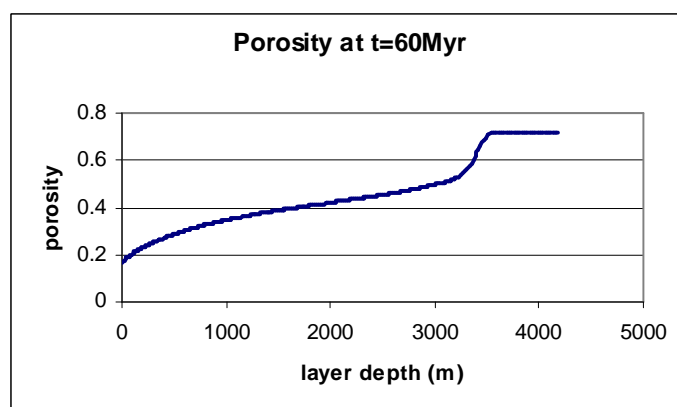


Figure 7: Porosity versus layer depth at  $t=60$ Myr.

The hydromechanical boundary conditions are showed in Fig. 8. The lateral right-hand side (resp. left-side) is subjected to a constant horizontal velocity  $V \underline{e}_x$  (resp.  $-V \underline{e}_x$ ). Only the results related to contractional motion will be provided in the sequel (i.e.,  $V < 0$ ). Two

typical values for the prescribed velocity magnitude are considered:  $V = -1 \text{ cm/year}$  (fast tectonics) and  $V = -0.5 \text{ mm/year}$  (slow tectonics).

It is recalled that the mesh for tectonic simulations is the deformed mesh of that described in section 4 and considered for the simulation of basin during sediments deposition  $0 \leq t \leq 60 \text{ Myr}$ .

The fluid boundary conditions maintain the sediments in a fully saturated condition everywhere. The sides and the bottom of the model are impermeable. The upper surface of the model is infinitely permeable: water may enter or leave in this frontier.

The tectonic loading starts at  $t = T$  and the results will conveniently given in terms of displacement increment  $\underline{U}$  of the skeleton particles between the initial configuration at time  $T$  and the current configuration at time  $T + \Delta t$ , and pore pressure difference  $P$  at points similar within the skeleton transformation between  $T$  and  $T + \Delta t$ .

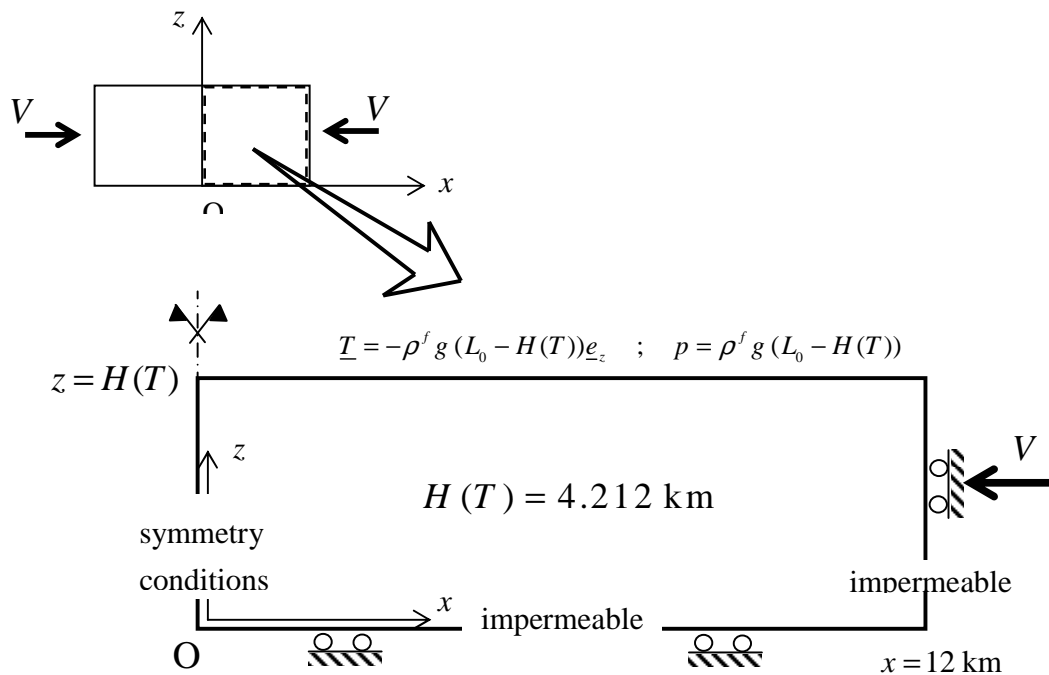


Figure 8: Initial geometry model and boundary conditions for tectonic simulations.

It is worth noting that the objective of this first approach is only to investigate the feasibility of the 2D modeling and not to provide quantitative insights in the basin deformation under tectonic loading.

At this stage, two fundamental questions can be already raised as regards the numerical modeling. Firstly, the boundary condition of frictionless at the basin basement is not very realistic and thus results in a more deformable block. Secondly, the shape quality of the

mesh elements resulting from compaction (vertical stretching) between  $t=0$  and  $t=T$  is rather low: due to oedometric contraction, the elements become thin with high aspect ratio. This is clearly the source of numerical inaccuracies and can lead to non numerical convergence.

## 5.2 Numerical results

### 5.2.1 Fast compressive tectonic motion

This situation corresponds to a lateral compression of the basin with velocity  $V = -1 \text{ cm/year}$ . The tectonic loading process is applied by increasing in time the prescribed horizontal displacement. The study was restricted to total duration  $\Delta t = 1495 \text{ years}$ , which corresponds to a total prescribed displacement of  $-14.95 \text{ m}$ . This corresponds of course to a moderate amount of lateral extension. Actually, numerical convergence of the procedure is not obtained for further values of prescribed displacement. The configuration reached after  $\Delta t = 1495 \text{ years}$  will be referred to as failure configuration.

In its current state of development, the numerical procedure is not able to simulate the evolution of the basin for times  $\Delta t > 1495 \text{ years}$ . It is likely that two phenomena contribute to 'the appearance' of this failure configuration. First, as a consequence of the numerical shortcomings emphasized at the end of section 5.1 and it would be the expression of rather a 'numerical failure' than a physical failure. Secondly, this failure can be explained as follows. Fast contractional tectonic induces high pore pressure in undrained-like conditions, which in turn lead rapidly to substantial increase in the effective stresses controlling the yield failure.

Increment of displacement, pore pressure and earth pressure coefficient induced by tectonic motion are showed in the sequel (Figs. 9-13). While gravitational compaction does not induce any horizontal displacement (oedometric conditions), that induced by tectonic loading is as expected is of decreasing magnitude as moving toward the symmetry plane  $x=0$  of the basin. As regards the vertical displacement, Fig. 10 shows that tectonic loading slightly affects this component which is mainly due to pore pressure dissipation process. The velocity field in the basin reported in Fig. 11 is typical of a failure mechanism defined by a localized failure zone developing from the basin basement to the symmetry plane. The final thickness of the basin at failure is about  $H=3554 \text{ m}$ , which corresponds to a compaction level of  $658 \text{ m}$  has occurred. It is worth observing that the magnitude of the considered fast tectonic motion is not enough to cause uplift of the basin.

In classical analyses, the coefficient of earth pressure is an important parameter in basin engineering. It is defined as the ratio between the horizontal and vertical effective stresses  $K_p = \frac{\sigma_h'}{\sigma_v'}$ . Based on heuristic elastic reasoning, a usual assumption in the field consists in considering the value of this parameter as constant in the basin at a given age. The profile of  $K_p$  along the mid-plane obtained from the numerical simulation is showed in Fig. 12. It turns out that, except in a thin crust near the upper surface of the basin, this parameter is quasi-constant. This result confirms thus the common practice which is to characterize a given basin by a single value of  $K_p$ . The distribution along the basin of the increment in pore pressure between  $T$  and  $T + 1495$  years is reported in Fig. 13.

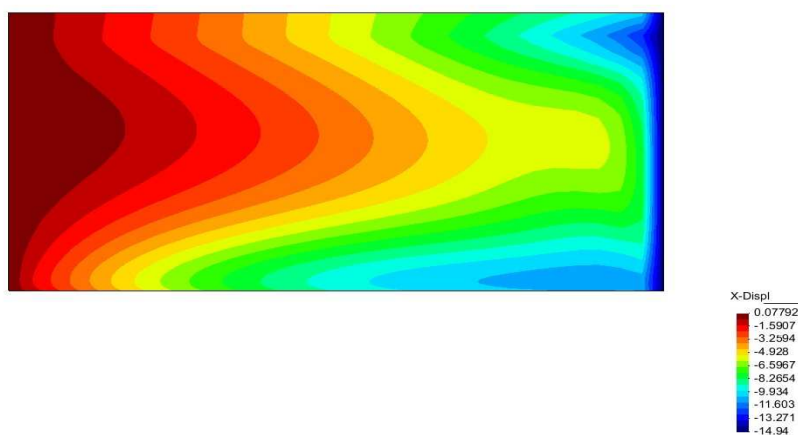


Figure 9: Contours fill of horizontal total horizontal displacement at failure  $\Delta t = 1495$  years .

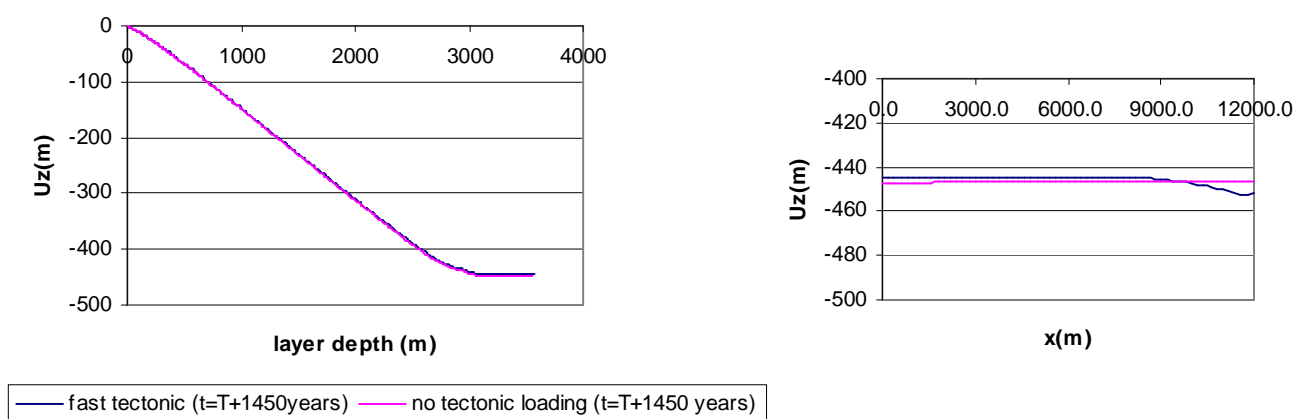


Figure 10: Vertical displacement along the basin plane  $x = 6\text{ km}$  and at to top of basin  $z = H$  after  $\Delta t = 1495$  years .

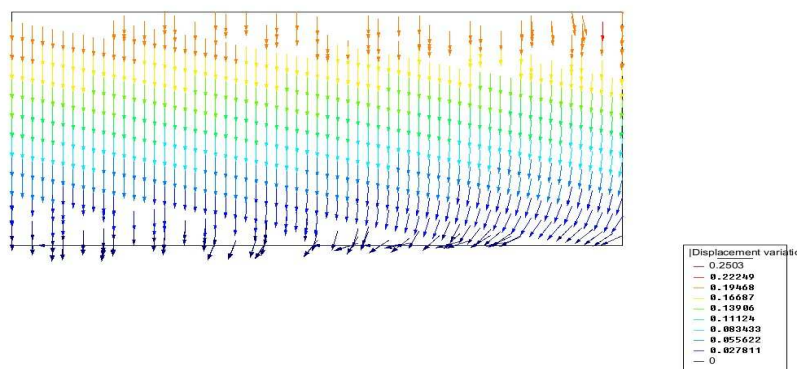


Figure 11: Velocity field at failure after  $\Delta t = 1495$  years .

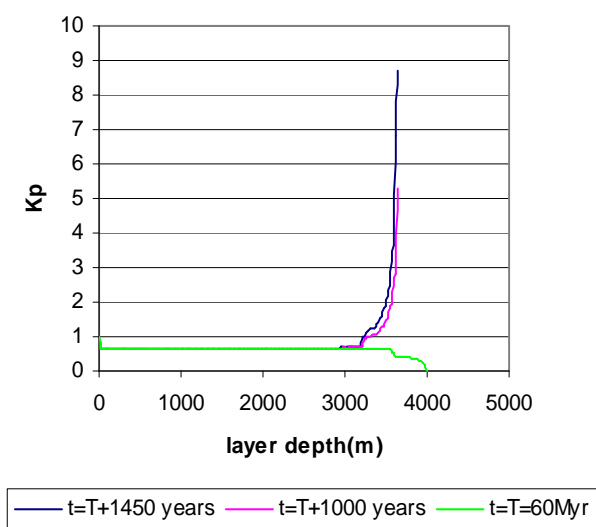


Figure 12: Coefficient of earth pressure  $K_p$  along the mid-plane  $x = 6$  km .

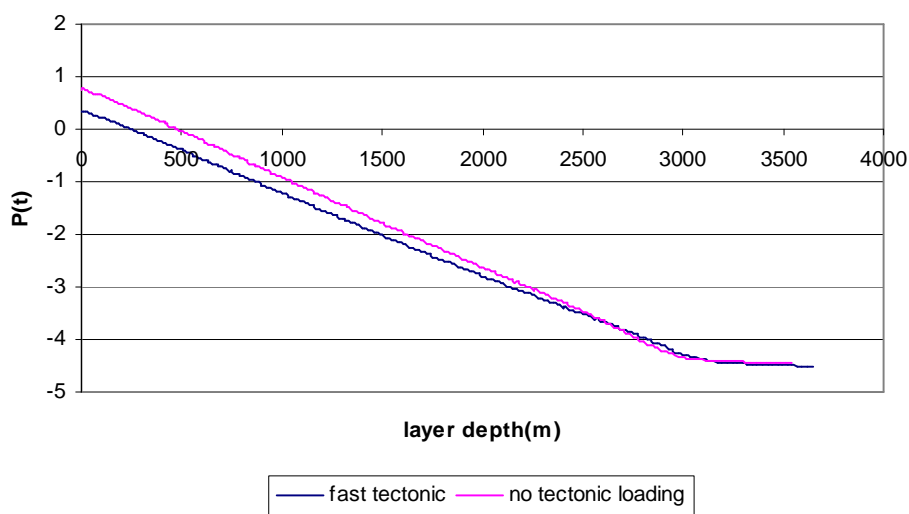


Figure 13: Pore pressure increment along the mid-plane  $x = 6$ km at failure  $\Delta t = 1495$  years .

### 5.2.2 Slow compressive tectonic motion

This situation corresponds to a contractional tectonic defined by a horizontal velocity equal to  $V = -0.5 \text{ mm/year}$ . Unlike the situation of fast tectonic motion, the basin deforms under drained-like conditions. This explains why failure only occurs after a significant amount of lateral extension. Failure, expressed herein by the non convergence of the numerical procedure, is after a total duration  $\Delta t = 126000 \text{ years}$  corresponding to a total prescribed displacement of  $-63 \text{ m}$ . Two opposite mechanisms control the basin deformation: that resulting from pore pressure dissipation due to gravitational compaction which causes downward displacement and that induced by horizontal forces due tectonic loading which causes upward displacement. The net result in the present case is an uplift of the basin. Increment of displacement, pore pressure and earth pressure coefficient induced by tectonic motion are showed in the sequel (Figs. 14-18).



Figure 14: Contours fill of total horizontal displacement at failure  $\Delta t = 126000 \text{ years}$ .

## 6 CONCLUSIONS

A constitutive model has been formulated for the sedimentary basin. It aims at incorporating some of the fundamentals coupled phenomena involved in the process of basin compaction and tectonic activity by means of a simplified micro-to-macro framework. The magnitude of porosity changes induced by compaction imposes to adopt the framework of finite poroplasticity. The derived model is able to account for the stiffness

increase and for the corresponding variation of pore volume. An important feature of this model is that the expression of the hardening law avoids development of negative porosities that are encountered with classical models of the Clam-Clay type.

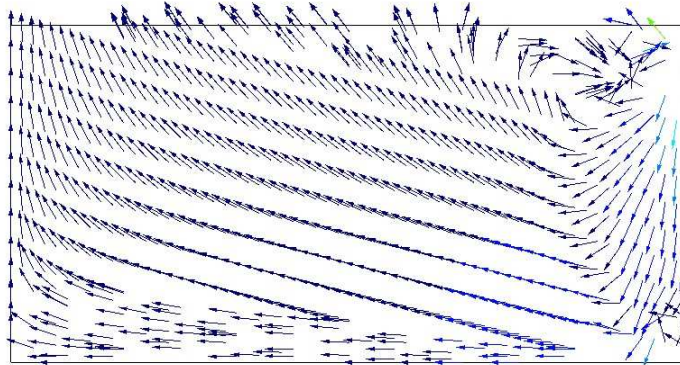


Figure 15: Velocity field at failure after  $\Delta t = 126000$  years .

From numerical point of view, a finite element formulation using updated Lagrangian scheme is implemented in order to analyze the time dependent large deformation of the poroplastic basin.

A numerical approach to the process of sediment accretion has been proposed: its principle consists in replacing the open material system (i.e., the basin) into a fictitious closed one, and to model the phases of sediments deposit-erosion by activating-deactivating the sub-layers. These theoretical and numerical developments have been implemented in a finite element code.

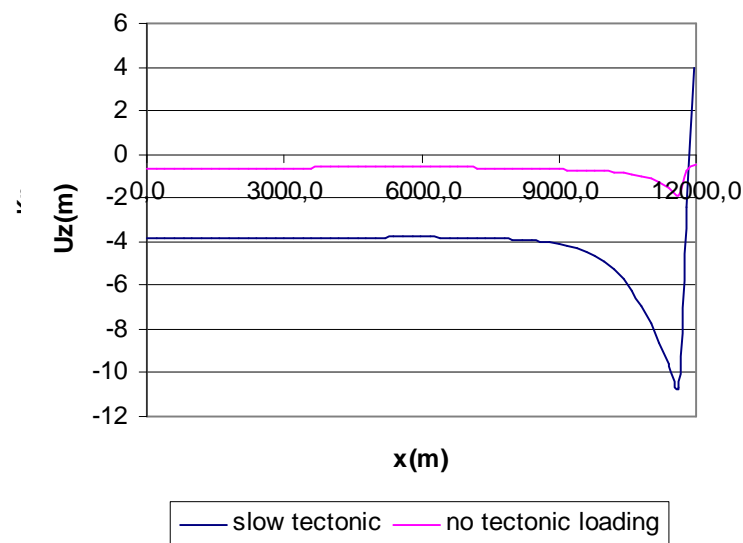


Figure 16: Vertical displacement at the top of the basin.

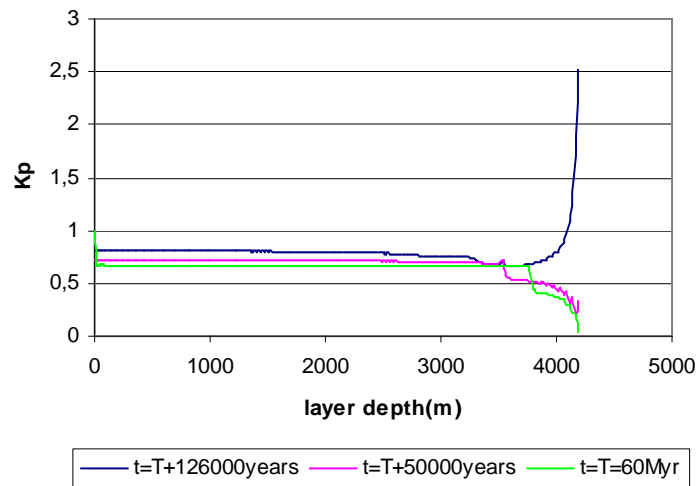


Figure 17: Coefficient of earth pressure  $K_p$  along the mid-plane  $x = 6\text{ km}$ .

The tectonic calculations have been performed with a 2D model taking as configuration that obtained after phase of sediments deposition (i.e., end of the basin construction), which means that the porosity, Young’s modulus and hardening parameter varies with the layer depth. The tectonic modeling is performed with an imposed displacement at the right side of the basin and we studied here only a tectonic compression. For the parameters used in the tectonic calculations, the maximum displacement is always the vertical one (due to compaction), the horizontal displacement are quite small compared with the vertical ones. Nevertheless, it is found that in case of slow tectonic motion, the basin can undergo an uplift induced by the horizontal forces.

Conceptually, the numerical tool under its current form can be adopted to simulate basins undergoing three-dimensional evolutions of the type induced by a tectonic loading. However, the increase of the number of degrees of freedom requires to develop more efficient numerical strategies including parallel computing.

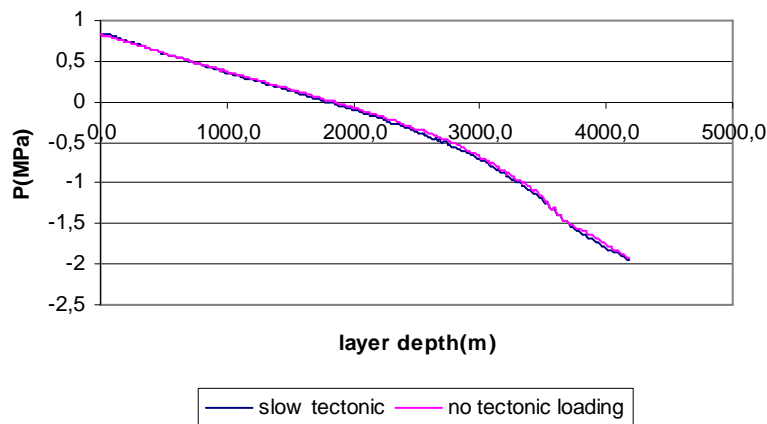


Figure 18: Pore pressure increment along the mid-plane  $x = 6\text{ km}$  at failure  $\Delta t = 126000\text{ years}$ .

## REFERENCES

- Babeyko A.Y., Sobolev S.V., Trumball R.B., Onken O. and Lavier L.L. Numerical models for crustal scale convection and partial melting beneath the Altiplano-Puna plateau. *Earth and Planetary Sciences Letters*, 199:373-388, 2002.
- Bathe K.J. *Finite element procedures in engineering analysis*. Englewood Cliffs, Prentice-Hall, 1996.
- Barnichon J. D. and Charlier R. Finite element modeling of the competition between shear bands in the early stages of thrusting: strain localization analysis and constitutive law influence, Buchanan PG, Nieuwland DA editors. Modern developments in structural interpretation, validation and modeling, *Geol Soc London Spec Publ*, 99:235-250, 1996.
- Barthélémy F.F., Dormieux L. and Maghous S. Micromechanical approach to the modelling of compaction at large strains. *Computers and Geotechnics*, 30:321-338, 2003.
- Bernaudo D., Deudé V., Dormieux L., Maghous S. and Schmitt D.P. Evolution of elastic properties in finite poroplasticity and finite element analysis. *Int. Journal Anal Meth Geomech*, 26(9):845-871, 2002.
- Bernaudo D., Dormieux L. and Maghous S. A constitutive and numerical model for mechanical compaction in sedimentary basins. *Computers and Geotechnics*, 33: 316-329, 2006.
- Bourgeois E. and Dormieux L. Prise en compte des non-linéarités géométriques dans la modélisation de la compaction de sédiments. *Oil Gas Sci Technol-Rev l'IFP*, 52(1):23-34, 1997.
- Bourgeois E., de Buhan P. and Dormieux L. Derivation of an elastoplastic constitutive law for saturated porous media at finite strains. *CR Acad Sci, Paris*, 321(IIb):175-182, 1995.
- Buiter S.J.H., Pfiffner O. A. and Beaumont C. Inversion of extensional sedimentary basins: A numerical evaluation of the localization of shortening. *Earth and Planetary Science Letters*, 288:492-504, 2009.
- Deudé D., Dormieux L., Maghous S., Barthélémy J.F. and Bernaudo D. Compaction process in sedimentary basins: the role of stiffness increase and hardening induced by large plastic strains. *Int J Numer Anal Meth Geomech*, 28:1279-1303, 2004.
- Dormieux L. and Maghous S. Poroelasticity and poroplasticity at large strains. *Oil Gas Sci Technol-Rev l'IFP*, 54:773-784, 1999.
- Dormieux L. and Maghous S. Evolution of elastic properties in finite poroplasticity. *CR Acad Sci, Paris*, 328(IIb):593-600, 2000.
- Frederiksen S., Nielsen S.B. and Balling N. A numerical dynamic model for the

- Norwegian-Danish basin. *Tectonophysics*, 343:165-83, 2001.
- Hubert M.K. and Rubey W.W. Role of fluid pressure in mechanics of overthrust faulting, I. mechanics of fluid-filled porous solids and its application to overthrust faulting. *Bull Geol Soc Am*, 70:115-166, 1959.
- Hutton E.W.H. and Syvitski J.P.M. Advances in the numerical modeling of sediment failure during the development of a continental margin. *Marine Geology*, 203:367-380, 2004.
- Jarosinski M., Beekman F., Matenco L. and Cloetingh S. Mechanics of basin inversion: Finite element modeling of the Pannonian Basin System. *Tectonophysics*, 2009.
- Mantovani E. Viti M., Albarello D., Tamburelli C., Babbucci D. and Cenni N. Role of kinematically induced horizontal forces in Mediterranean tectonics: insights from numerical modeling. *Journal of Geodynamics*, 30:287-320, 2000.
- Mello U.T., Rodrigues J.R.P. and Rossa A.L. A control-volume finite-element method for three-dimensional. *Marine and Petroleum Geology*, 26:504-518, 2009.
- Meroi E.A., Schrefler B. and Zienkiewicz O. Large strain static and dynamic semisaturated soil behaviour. *Int J Numer Anal Meth Geomech*, 19:81-106, 1995.
- Muir W.D.M. Soil behavior and critical state soil mechanics. *Cambridge University Press*, 1990.
- Schmidt V. and Mc Donald D.A. The role of secondary porosity in the course of sandstone diagenesis. Scoble PA, Schlugger PR, editors. Aspects of diagenesis, *Society of economic paleontologists and mineralogists special publication*, 26:175-207, 1979.
- Smith J. E. The dynamics of shale compaction and evolution of fluid pressures. *Math Geol*, 3(3):239-263, 1971.
- Strayer L.M., Hudleston P.J. and Lorig L.J. A numerical model of deformation and fluid flow in an evolving thrust wedge. *Tectonophysics*, 335:121-145, 2001.
- Tuncay K., Park A. and Ortoleva P. Sedimentary basin deformation: an incremental stress approach. *Tectonophysics*, 323:77-104, 2000.
- Zaoui A. Continuum micromechanics: survey. *J Eng Mech*, 128(8):808-816, 2002.
- Zhao C., Hobbs B.E., Walshe J.L., Mühlhaus H.B. and Ord A. Finite element modeling of fluid-rock interaction problems in pore-fluid saturated hydrothermal/sedimentary basins. *Comput Meth Appl Mec . Engrg*, 190:2277-2293, 2001.